Optical Characterization of Double-Wall Carbon Nanotubes: Evidence for Inner Tube Shielding

Konstantin Iakoubovskii, Nobutsugu Minami,* Taro Ueno, Said Kazaoui, and Hiromichi Kataura

Nanotechnology Research Institute, National Institute of Advanced Industrial Science and Technology (AIST), 1-1-1 Higashi, Tsukuba, 305-8565, Japan

Received: March 2, 2008; Revised Manuscript Received: April 12, 2008

This paper presents a comprehensive optical study of double-wall carbon nanotubes (DWNTs) grown by chemical vapor deposition, using optical absorption, photoluminescence (PL), and Raman spectroscopies. Extending the spectral ranges of absorption and PL measurements beyond 2300 nm made it possible to detect signals both from the inner and the outer shells of DWNTs. Application of in situ perturbations, namely, oxidation with light-generated ozone and electrochemical doping, unambiguously proved the double-wall structure of our samples and revealed the efficient shielding of the inner DWNT shells by the outer shells. Analysis of the absorption spectra measured under progressive ozone oxidation allowed us to decompose the total DWNT absorption into the contributions from the inner and outer shells and to estimate the filling ratio of DWNTs.

Introduction

Double-wall carbon nanotubes (DWNTs) are a fascinating object, studying which we can greatly enhance our understanding of single-wall and multiwall carbon nanotubes (SWNTs and MWNTs). For example, by monitoring the response of the inner and outer shells of DWNTs to Br_2 exposure it was found[1,2] that it is the outer, not the inner, surface of the nanotube that reacts with bromine (and possibly with other gases); nuclear magnetic resonance studies of ^{13}C-enriched DWNTs revealed an unusual metallic behavior of the inner shells in peapod-derived DWNTs.[3] Besides, monitoring the interaction between the inner and outer shells in a DWNT allows us to study intermolecular interactions. For example, Raman measurements on peapod-derived DWNTs revealed narrow-line structure of radial breathing modes (RBMs), which was successfully explained in terms of the RBM shift due to variation in the distance between the inner and outer DWNT shells;[4] the shielding of the inner DWNT shells by the outer shells from applied pressure was also demonstrated by Raman scattering.[5]

Those examples are exciting, but their realization crucially relies on the thorough characterization of DWNTs and the detection of signals from both the inner and outer shells. Currently, there is a significant skepticism about the composition of the DWNT samples: it is known that they do contain SWNTs and MWNTs. The former (but not the latter) are known to produce relatively efficient optical (especially luminescence and Raman) signals, and therefore, in many instances it is unclear whether the detected signals originate from the major DWNT sample component or from minor SWNT fractions.

Raman spectroscopy and high-resolution electron microscopy (HREM) have been mainly applied for the DWNT characterization thus far. Those techniques are powerful, but they have clear disadvantages: HREM scans rather small sample volumes (of the order of cubic nanometers) and is therefore difficult to reliably correlate with other, macroscopic techniques due to the persistent sample inhomogeneity. As to Raman spectroscopy, it detects only a small fraction of nanotubes, those which resonantly absorb the excitation light and whose orientation is parallel to the polarization of the exciting laser. Consequently, sweeping the excitation in a wide range is necessary to characterize the structure of nanotube samples by Raman scattering, which is technically a daunting task requiring laser(s) tunable in a wide spectral range. Besides, most modern Raman spectrometers are microscope-based; they therefore probe only small sample volumes (approximately cubic micrometers) and thus again are prone to sample inhomogeneities.

On the contrary, photoluminescence (PL) excitation (PLE, also commonly referred to as "PL mapping") and optical absorption spectroscopies seem rather appropriate for the DWNT characterization for at least three reasons: they can easily scan large sample volumes (approximately cubic millimeters) and thus do not suffer from sample inhomogeneity; they are relatively simple and widely available; the utilized light source (lamp + monochromator) allows one to scan a wide excitation range thereby detecting most NTs.

Optical absorption applied to DWNTs detected signals both from the inner and the outer DWNT shells.[6–10] However, significant overlap has been revealed between these signals and their deconvolution has not been achieved yet. In the present work, application of ozone etching and electrochemical doping allowed us to separate absorption from the inner and outer DWNT shells. On the other hand, PL usually detected only the inner shells.[6,7] The limited PL detection range and interference by the solvent (D_2O) absorption hindered the detection of outer-shell signals in most studies (though see ref11). Both these problems have been solved in our recent reports: the solvent has been avoided by preparing dried, dense, optically homogeneous thin films of well-dispersed and purified nanotubes using carboxymethylcellulose[12] (CMC) or a combination of gelatin and sodium dodecylbenzene sulfonate[13] (SDBS) as dispersing media, and the PL detection range has been extended up to 2300 nm using a Fourier transform infrared (FTIR) spectrometer equipped with an IR-extended InGaAs detector.[13] These technical advances allowed us, in the present work, to

* Corresponding author. E-mail: n.minami@aist.go.jp.

10.1021/jp8018414 CCC: $40.75
Published on Web 07/02/2008

detect and unambiguously identify optical signals from both the inner and outer DWNT shells and to study the composition (in terms of the nanotube chiralities) of the both shells.

Experimental Section

DWNT Powders. The DWNT powders were produced by chemical vapor deposition from ethanol using Fe and MgO as catalysts. Note that these DWNTs have rather different properties from the peapod-derived DWNTs,[3,11] where the inner shell is formed by annealing C_{60} molecules encapsulated in SWNTs. The metal catalyst was etched away by acids. Residual SWNTs were removed by annealing at 500 °C in air for 30 min, as confirmed by optical measurements. The fraction of DWNTs in the powders was close to 100% as estimated by HREM measurements.

Sample Preparation. Optical absorption and Raman measurements were performed on "buckypapers" deposited on silica substrates. The buckypapers were prepared by the vacuum filtration technique.[14] PL measurements were performed on films cast on silica from an SDBS dispersion mixed with 10% aqueous solution of gelatin, where gelatin's gelation helps to avoid nanotube aggregation during the drying.[13] Note that nanotube dispersion and the prevention of rebundling in the subsequent process is essential for PL studies, because PL is efficiently quenched in aggregated nanotubes. Dispersion was performed as follows: DWNT powders were dispersed for 30 min in 1% D_2O solution of SDBS using a tip sonifier (20 kHz, ~150 W). The dispersions were ultracentrifuged for 5 h, and the upper 80% supernatant was collected.

Measurements. All characterizations were performed at room temperature. Optical absorption was recorded with a commercial Shimadzu UV 3100PC double-beam spectrometer. Raman scattering measurements were performed with a Jasco NRS-2100 triple-grating spectrometer at 4 cm^{-1} resolution. He−Ne (633 nm) laser was employed for excitation. PL was measured with a home-built setup.[13] Excitation was provided by a tunable Ti:sapphire laser (695−1055 nm range) or a 300 W Xe lamp coupled to a 0.3 m monochromator (300−1600 nm range). Emission was detected either with an IR-extended FTIR system[13] (detection range 900−2300 nm, resolution 16 cm^{-1}) or with an InGaAs photodiode array (800−1600 nm) attached to a 0.3 m monochromator.

In situ UV illumination was provided with a low-pressure pen-shaped Hg lamp positioned at ~1 mm from the sample. This lamp mostly emits narrow lines at 185 and 254 nm and therefore, despite its low intensity (~1 mW/cm^2), is an efficient ozone generator. In order to check for possible light-induced, rather than ozone-related effects, test absorption and Raman measurements were performed where the lamp was significantly shifted from the sample (thus minimizing ozone etching), but the light intensity at the sample was kept unchanged by focusing. Those supposed light-induced effects appeared negligible, confirming that the observed effects were predominantly due to light-generated ozone.

Electrochemical doping was achieved under a potentiostatic condition using a DWNT film as a working electrode, which was prepared by spraying an ethanol dispersion of DWNT onto semitransparent, indium tin oxide (ITO)-coated glass substrates. A Pt electrode and an Ag wire were used as a counter and a quasi-reference electrode, respectively. Lithium perchlorate was dissolved in acetonitrile as a supporting electrolyte. Optical absorption due to acetonitrile was compensated by placing a reference cell into the reference beam of the absorption spectrometer.

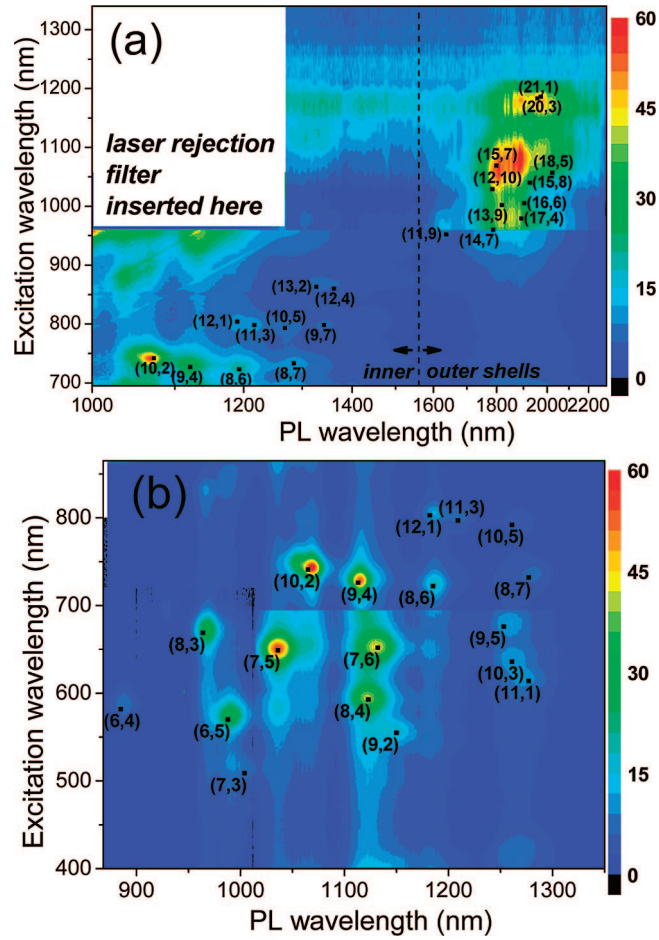

Figure 1. PL maps of a DWNT/SDBS/gelatin film measured with the IR-extended FTIR (a) and the photodiode array spectrometer (b).

Results and Discussion

PL Measurements. Figure 1 shows PL maps recorded from DWNT/SDBS/gelatin films. The (n, m) labeled squares present the conventional chirality assignment using the widely accepted data of Weisman and Bachilo,[15] which were slightly (by ~1%) offset in order to compensate for the matrix-induced peak shift. Those squares correspond to absorption into the second band gap S_{22} of semiconducting DWNTs followed by emission from the S_{11} states of the first band gap. Figure 1a presents an extended FTIR−PL map for a DWNT/SDBS/gelatin film. Note that the unassigned peaks in the excitation range of 850−950 nm and the detection range of 1000−1250 nm originate from S_{11} transitions from the narrow-diameter (inner-shell) tubes, excited not into S_{22} transitions, but into the phonon sidebands of the S_{11} peaks.[16] The low-wavelength region of the PL map measured with the InGaAs photodiode array is shown in detail in Figure 1b.

The pattern of (n, m) squares in Figure 1 reveals a bimodal nanotube diameter distribution with the maxima around 0.9 and 1.6 nm, in agreement with our previous result.[13] This bimodality could be considered as a strong evidence of the double-wall structure of the studied nanotubes. However, because a bimodal distribution has been reported for SWNTs as well,[17] further evidence of the double-wall structure will be given in the next section by introducing external perturbations, namely, UV illumination and electrochemical doping.

UV Illumination Effects. Figure 2 demonstrates the effect of in situ UV illumination on Raman and absorption spectra from DWNT buckypaper. Panel a presents Raman spectra in

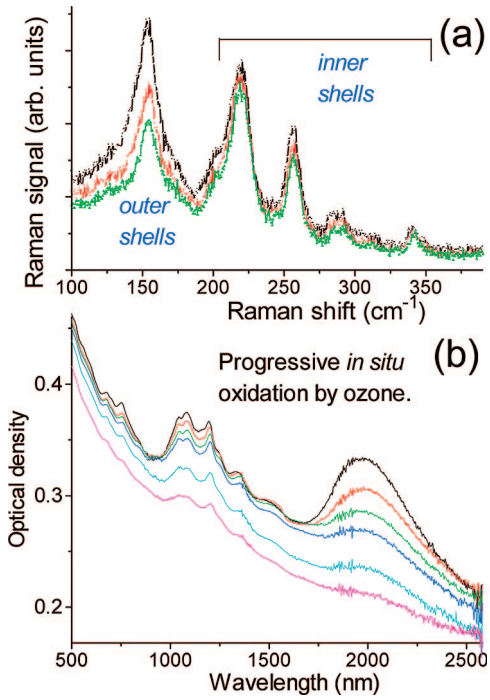

Figure 2. Raman (panel a; 633 nm excitation, RBM mode region) and optical absorption (b) spectra from a DWNT buckypaper measured under progressing in situ oxidation by ozone generated by a low-power UV lamp. The irradiation time is, from the top spectrum to bottom, 0, 5, and 10 min for panel a and 0, 3, 6, 10, 20, and 40 min for panel b. The irradiation intensity was similar, but not identical, for panels a and b.

the RBM region. The RBM mode frequency is uniquely associated with the nanotube diameter, and thus the Raman peaks at ~150 and at 200−350 cm^{-1} in Figure 2a can be attributed to the outer and inner shells, respectively. Within this assignment, the Raman scattering results of Figure 2a can be described as that UV illumination significantly (and irreversibly) reduces the signals from the outer shells, whereas the inner shells undergo relatively small change. This behavior is logically expected for DWNTs and is inconsistent with the SWNT structure. The mechanism behind the UV-induced changes in Raman spectra could be the generation of ozone by UV light followed by the preferential ozone etching of the outer DWNT shells.

In addition to Raman experiments, the in situ ozone-induced oxidation of DWNT buckypapers was also performed in absorption measurements (see Figure 2b). The spectra show that by progressive oxidation the absorption intensity decreases over the entire wavelength range, but the change is much faster at 2000 nm than at 1200 nm. This is again consistent with the double-wall structure, where the outer tubes are etched away faster than the inner tubes. Note that the 1200 nm peaks also decrease albeit rather slowly. This is so because at this wavelength two optical transitions, namely, S_{11} transitions in the inner tubes (S^{i}_{11}) and S_{22} transitions in the outer tubes (S^{o}_{22}) overlap.[8−10] The etching of the outer tubes with the inner tubes kept almost intact results in the partial and slower reduction of the absorption at 1200 nm, in contrast with the complete disappearance of the 2000 nm peak originating solely from the S^{o}_{11} transitions in the outer tubes. This could be another manifestation of the shielding of the inner tubes by the outer tubes.

Figure 3 reveals that UV illumination also drastically alters the PL spectra from a DWNT/SDBS/gelatin film excited at 940 nm: the PL peak at 1800 nm deriving from the outer shells significantly decreased, whereas that at 1200 nm from the inner shells underwent very little change. Note here that the latter PL emission originates from the excitation of the phonon sidebands of the S_{11} peaks of the inner shells, not from the S_{22} excitation. The reason for quenching of PL in DWNT/SDBS/gelatin films by UV illumination is yet uncertain, but it could be tentatively attributed to UV-induced interactions between the DWNTs and the SDBS/gelatin matrix.[18] Presence of the (SDBS/gelatin) matrix crucially distinguishes the UV-induced effects in PL from those in absorption or Raman. In the latter experiments, pure buckypapers have been used, and the UV effects could be reasonably associated with ozone-induced etching.

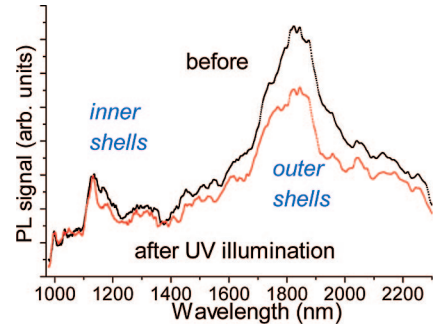

Figure 3. FTIR−PL spectra from a DWNT/SDBS/gelatin film measured under 940 nm excitation, before and after UV illumination. There is a noticeable (and irreversible) decrease in the signals assigned to the outer shells, but not from the inner shells.

Electrochemical Doping. To assert the effect of inner tube shielding we performed in situ electrochemical doping, where electron depletion from the valence bands under the anodic polarization of the DWNT electrode was monitored by absorption measurements. For comparison, two separate SWNT samples were also used, namely, the one produced by laser ablation (LA-SWNT) and the other HiPco-SWNT (CNI). Note that the diameter of the former is close to that of the outer tube of DWNT and that of the latter close to the inner tube, which facilitates their comparison.

The results are summarized in Figure 4. For DWNT (panel a), the increase in the anodic polarization depletes the peak at 2000 nm first and then those at 1000−1400 nm. Note, however, that even at the potential of 1.2 V (vs Ag wire), the latter peaks still persist. For LA-SWNT (panel b), in contrast, all the main peaks completely disappear at 1.2 V, which means that, for SWNTs with diameters similar to the outer tubes of DWNTs, this potential is strong enough to deplete all the valence electrons contributing to S_{11} and S_{22} transitions. A logical conclusion is that the residual absorption peaks at 1.2 V observed for DWNT originate from the (shielded) inner tubes. Further evidence for shielding is provided by the result for HiPco-SWNT (panel c), where again all the absorption peaks completely disappear at 1.2 V. This confirms that shielding by the outer tubes is necessary to prevent the valence electron depletion in carbon nanotubes (CNTs) of this diameter. The results of electrochemical doping in combination with those of ozone etching have unambiguously established the double-wall structure and the shielding effect. Note that an electrochemical modulation of DWNT absorption has been reported already,[8] however, without reference SWNT measurements. Consequently, those changes could well be interpreted as originating from SWNTs of different diameters rather than DWNTs.

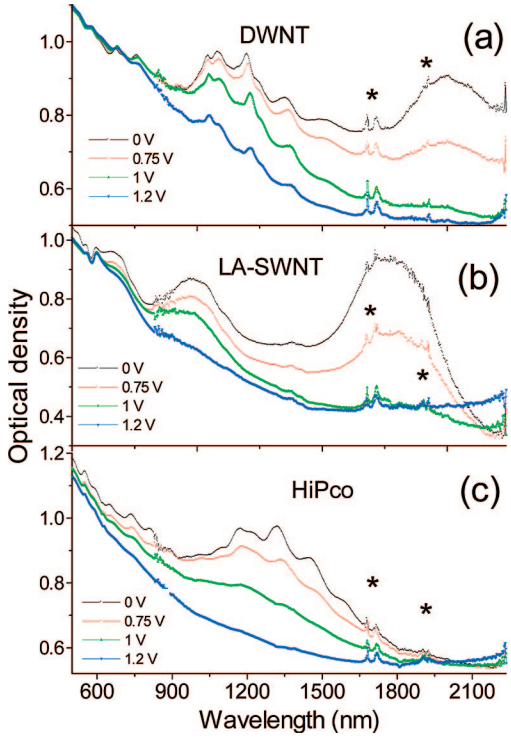

Figure 4. Absorption spectra from DWNT (a), laser-ablation-SWNT (b), and HiPco-SWNT films (c) prepared by spraying on ITO substrates, measured under progressive electrochemical doping. Asterisks mark sharp absorption peaks of acetonitrile.

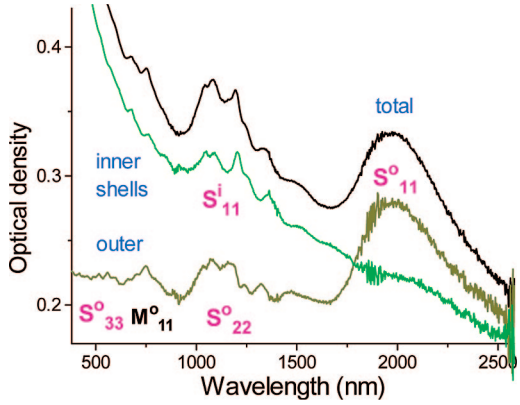

Figure 5. Decomposition of the optical absorption spectra from a DWNT buckypaper into the outer- and inner-shell contributions, using the ozone etching procedure (see Figure 2b).

Analysis of the Optical Absorption Spectra from DWNTs. On the basis of the results of Figure 2 we might reasonably assume that the initial ozone oxidation stage shown in the top two spectra in Figure 2b affects only the outer, but not the inner shells. Therefore, the difference between the two spectra specifically reflects the absorption spectrum of the outer tubes. By subtracting this difference from the initial DWNT spectrum in Figure 2b, one could in principle extract the inner tubes' absorption spectrum. Before the subtraction, the difference spectrum is multiplied by an appropriate factor, so the final spectrum contains no feature at 2000 nm, at which wavelength no absorption is expected for the inner tubes. The results of such analysis are shown in Figure 5, where the total spectrum is deconvoluted into the inner and outer tubes' contributions. Progressing toward shorter wavelength, the outer tubes exhibit a series of structured bands, which are traditionally assigned to the S_{11}, S_{22}, M_{11}, and S_{33} transitions.[15] Here M_{11} refers to the first band gap of the metallic nanotubes. Interestingly, we can estimate the filling percentage of DWNT, namely, the length ratio of the inner tubes versus the outer, from the integrated ratio of S^i_{11}/S^o_{11} bands. After replotting Figure 5 in an energy scale and subtracting linear baselines from the corresponding bands, the integrated S^i_{11}/S^o_{11} ratio was estimated as 90% ± 10%, which is consistent with HREM observations.

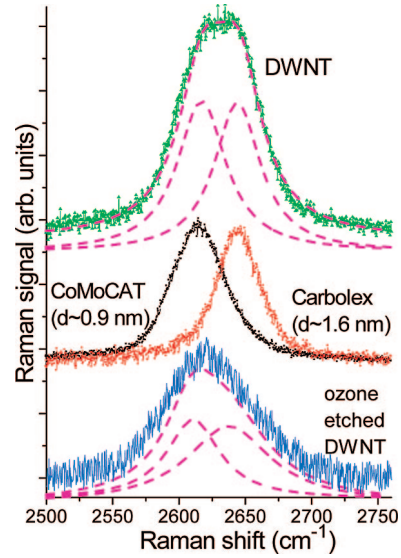

Figure 6. Raman spectra (633 nm excitation) of the G′ modes in DWNTs (top green curve) and reference CoMoCAT ($d \sim 0.9$ nm) and Carbolex ($d \sim 1.6$ nm) SWNTs (middle curves). The bottom blue curve is a spectrum of the DWNT after ozone oxidation of the outer shells. It corresponds to the bottom curve in Figure 2b. Dashed lines present decompositions into Lorentzian components. The spectra are vertically shifted for presentation purpose.

The G′ Raman Mode. The top curve of Figure 6 shows the spectrum of the G′ Raman mode in DWNT buckypaper. It reveals an unresolved doublet structure as indicated by the Lorentzian decomposition (dashed lines). Note that the G′ name was given to this mode because it is the second strongest mode in graphite after the G mode ("G" from graphite); however, G′ is actually a second-order peak of the defect-induced D mode. The latter is (partially) forbidden and is therefore weak.

The first important feature of the G′ and D modes is that contrary to the RBM mode, their intensity is almost independent of the excitation energy, i.e., a single laser line will excite the G′ and D modes in most of the nanotubes. Another peculiarity of the G′ and D modes is that their peak positions depend on the nanotube diameter.[19] The dependence is, however, stronger for the G′ than for the D mode; besides, the G′ mode intensity is stronger. Therefore, this mode can be conveniently used to monitor the diameter distribution of the nanotubes. Indeed, the middle curves in Figure 6 demonstrate a clear difference in the peak position of the G′ mode in the commercial CoMoCAT ($d \sim 0.9$ nm) and Carbolex ($d \sim 1.6$ nm) SWNTs. Those SWNTs serve here as references for the inner and outer tubes of our DWNTs. Although we used LA-SWNT and HiPco-SWNT references above, the differences between CoMoCAT and HiPco or Carbolex and LA-SWNTs are unessential here. Note the similarity between the decomposed DWNT G′ spectrum and the CoMoCAT and Carbolex spectrum. This result may be interpreted as that our DWNTs consist of two types of nanotubes with the mean diameters of ~0.9 and ~1.6 nm.

The bottom curve in Figure 6 presents the G′ mode spectrum in the DWNTs after their outer shells have been etched by UV-light-generated ozone. It corresponds to the bottom curve in

Figure 2b. An apparent shift of the G′ mode toward the low wavenumbers is observed. It is important to note that the G′ mode intensity is proportional not to the density of nanotubes but to the density of defects in the nanotubes, and therefore its interpretation is ambiguous. However the bottom spectrum of Figure 6 is consistent with the following scenario: Ozone treatment etched away most of the outer tubes and severely damaged those which were still left; this has broadened the contribution from the outer tubes but did not alter much its integrated intensity. Meanwhile, the inner tube signals were mostly unaffected, apart maybe from a minor intensity decrease.

Summary and Conclusions

This paper presented a comprehensive optical characterization of DWNTs. Extending the PL excitation and detection ranges into the IR region, combined with an appropriate sample preparation (well-dispersed nanotubes in a solvent-free film), allowed us to measure bimodal PL excitation maps composed of signals from the inner and outer DWNT shells. It is demonstrated that optical absorption spectra are an efficient monitor of the DWNT sample quality and of the diameter distributions of the inner and outer DWNT shells. Besides, they provide a valuable guide for choosing an appropriate excitation in Raman measurements.

In situ perturbations, namely, oxidation by light-generated ozone and electrochemical doping, have been applied to DWNTs in absorption, PL, and Raman experiments. They proved the double-wall structure of our samples and unambiguously revealed the shielding of the inner shells by the outer shells from those perturbations. Analysis of the Raman G′ mode and of the absorption spectra measured under progressive ozone oxidation allowed us to decompose the DWNT signals into the contributions of the inner and outer shells and to estimate the filling ratio of DWNTs. It is important to note that this study provided a simple and comprehensive analysis routine not only for DWNTs but also for multiwall carbon and noncarbon nanotubes.

References and Notes

(1) Souza Filho, A. G.; Endo, M.; Muramatsu, H.; Hayashi, T.; Kim, E. A.; Barros, E. B.; Akuzawa, N.; Samsonidze, Ge. G.; Saito, R.; Dresselhaus, M. S. *Phys. Rev. B* **2006**, *73*, 235413.

(2) Chen, G.; Bandow, S.; Margine, E. R.; Nisoli, C.; Kolmogorov, A. N.; Crespi, V. H.; Gupta, R.; Sumanasekera, G. U.; Iijima, S.; Eklund, P. C. *Phys. Rev. Lett.* **2003**, *90*, 257403.

(3) Singer, P. M.; Wzietek, P.; Alloul, H.; Simon, F.; Kuzmany, H. *Phys. Rev. Lett.* **2005**, *95*, 236403.

(4) Pfeifer, R.; Simon, R.; Kuzmany, H.; Popov, V. N. *Phys. Rev. B* **2005**, *72*, 161404(R).

(5) Arvanitidis, J.; Christofilos, D.; Papagelis, K.; Andrikopoulos, K. S.; Takenobu, T.; Iwasa, Y.; Kataura, H.; Ves, S.; Kourouklis, G. A. *Phys. Rev. B* **2005**, *71*, 125404.

(6) Hertel, T.; Hagen, A.; Talaev, V.; Arnold, K.; Henrich, F.; Kappes, M.; Rosenthal, S.; McBride, J.; Ulbricht, H.; Flahaut, E. *Nano Lett.* **2005**, *5*, 511.

(7) Kishi, N.; Kikuchi, S.; Ramesh, P.; Sugai, T.; Watanabe, Y.; Shinohara, H. *J. Phys. Chem. B* **2006**, *110*, 24816.

(8) Kalbac, M.; Kavan, L.; Zukalova, M.; Dunsch, L. *Adv. Funct. Mater.* **2005**, *15*, 418.

(9) Gruneis, A.; Rummeli, M. H.; Kramberger, C.; Barreiro, A.; Pichler, T.; Pfeifer, R.; Kuzmany, H.; Gemming, T.; Buchner, B. *Carbon* **2006**, *44*, 3177.

(10) Bandow, S.; Hirahara, K.; Hiraoka, T.; Chen, G.; Eklund, P. C.; Iijima, S. *MRS Bull.* **2004**, *4*, 260.

(11) Okazaki, T.; Bandow, S.; Tamura, G.; Fujita, Y.; Iakoubovskii, K.; Kazaoui, S.; Minami, N.; Saito, T.; Suenaga, K.; Iijima, S. *Phys. Rev. B* **2006**, *74*, 153404.

(12) Minami, N.; Kim, Y.; Miyashita, K.; Kazaoui, S.; Nalini, B. *Appl. Phys. Lett.* **2006**, *88*, 93123.

(13) Iakoubovskii, K.; Minami, N.; Kazaoui, S.; Ueno, T.; Miyata, Y.; Yanagi, K.; Kataura, H.; Ohshima, S.; Saito, T. *J. Phys. Chem. B* **2006**, *110*, 17420.

(14) Hennrich, F.; Lebedkin, S.; Malik, S.; Tracy, J.; Barczewski, M.; Rösner, H.; Kappes, M. *Phys. Chem. Chem. Phys.* **2002**, *4*, 2273.

(15) Weisman, R. B.; Bachilo, S. M. *Nano Lett.* **2003**, *3*, 1235.

(16) Chou, S. G.; Plentz, F.; Jiang, J.; Saito, R.; Nezich, D.; Ribeiro, H. B.; Jorio, A.; Pimenta, M. A.; Samsonidze, G. G.; Santos, A. P.; Zheng, M.; Onoa, G. B.; Semke, E. D.; Dresselhaus, G.; Dresselhaus, M. S. *Phys. Rev. Lett.* **2005**, *94*, 127402.

(17) Okazaki, T.; Saito, T.; Matsuura, K.; Ohshima, S.; Yumura, M.; Oyama, Y.; Saito, R.; Iijima, S. *Chem. Phys. Lett.* **2006**, *420*, 286.

(18) Iakoubovskii, K.; Minami, N.; Kim, Y.; Miyashita, K.; Kazaoui, S.; Nalini, B. *Appl. Phys. Lett.* **2006**, *89*, 173108.

(19) Pimenta, M. A.; Jorio, A.; Brown, S. D. M.; Souza Filho, A. G.; Dresselhaus, G.; Hafner, J. H.; Lieber, C. M.; Saito, R.; Dresselhaus, M. S. *Phys. Rev. B* **2001**, *64*, 041401.

JP8018414